On the LuGre Model and Friction-Induced Hysteresis

Ashwani K. Padthe, JinHyoung Oh, and Dennis S. Bernstein
Department of Aerospace Engineering, The University of Michigan,
Ann Arbor, MI 48109-2140, USA, {akpadthe,johzz,dsbaero}@umich.edu

Abstract— **In this paper we study hysteresis induced by friction in a simple mass-spring system and then in a dc servo motor experimental setup. The experimental setup is modeled and simulated using the Dahl, LuGre, and Maxwell-slip friction models. Comparison of the experimental and simulation results reveals that the LuGre model provides the best model of the testbed's friction-induced hysteresis.**

I. Introduction

Modeling and control of friction remains a problem of interest, both for its intellectual challenge and its practical ramifications [1]–[3]. In recent work [4] we considered the relationship between friction models and hysteresis in mechanical systems. In particular, by using the results in [5] on Duhem models for hysteresis, we classified the most widely used friction models in terms of the properties of the relevant Duhem model; see Table 1.

In the present paper we extend the results of [4] in several directions. First, we more closely examine the nature of the hysteresis maps that arise from each friction model. This examination allows us to compare the hysteretic response of each friction model with the extensive experimental studies of friction models available in the literature [6]–[10]. Next, we embed each friction model within a single-degree-of-freedom mechanical model in order to examine and compare the hysteretic response of the system.

Finally, we develop an experimental testbed for friction identification. The testbed consists of a dc motor with a speed reduction gearhead, with encoder measurements of the shaft and load cell measurements of a cable wound around the gearhead. By operating this testbed under quasi static conditions, we compare its hysteretic response to the simulated response of the system under various friction models. The goal is to determine the most suitable friction model for the friction and stiction effects observed in the testbed. As the title of this paper suggests, the LuGre friction model, which exhibits stick-slip friction, is found to provide the best model of the testbed's hysteretic dynamics.

The contribution of the present paper is a broad, system-theoretic picture of various friction models and their induced hysteresis maps. All of the principal friction maps are studied in a common setting, and the resulting characteristic hysteresis maps are compared. While friction is known to be a source of hysteresis [8], [9], [11], our goal is to systematically examine the link between the physical phenomenon of friction and the system-theoretic phenomenon of hysteresis.

In Section 2 we review the analysis from [4] of the Dahl, LuGre, and Maxwell-slip friction models concerning their hysteretic characteristics. In Section 3 we study the friction-induced hysteresis in the mass-spring system using the three friction models. In Section 4 we develop a model of the experimental setup used for identifying friction. In Section 5 we simulate the model using the Dahl, LuGre, and Maxwell-slip friction models. In Section 6 we report the experimental results and compare them with the simulation results of Section 5. In Section 7 we give some concluding remarks.

II. Hysteresis in the Dahl, LuGre, and Maxwell-slip Friction Models

In this section, we review the Dahl, LuGre, and the Maxwell-slip friction models from a hysteresis modeling point of view as given in [4]. All the three friction models are expressed as Duhem models, thus indicating that friction can give rise to hysteresis. The terms closed curve, limiting periodic input-output map, hysteresis map, and rate-independence are defined in [5].

Consider the single-input single-output *generalized Duhem model* given by

$$\dot{x}(t) = f\big(x(t),u(t)\big)g\big(\dot{u}(t)\big), \qquad x(0)=x_0, \quad t\geq 0, \tag{1}$$

$$y(t) = h\big(x(t),u(t)\big), \tag{2}$$

where $x : [0,\infty) \to \mathbb{R}^n$ is absolutely continuous, $u : [0,\infty) \to \mathbb{R}$ is continuous and piecewise C^1, $f : \mathbb{R}^n \times \mathbb{R} \to \mathbb{R}^{n\times r}$ is continuous, $g : \mathbb{R} \to \mathbb{R}^r$ is continuous and satisfies $g(0) = 0$, $y : [0,\infty) \to \mathbb{R}$, and $h : \mathbb{R}^n \times \mathbb{R} \to \mathbb{R}$ is continuous. The value of $\dot{x}(t)$ at a point t at which $\dot{u}(t)$ is discontinuous can be assigned arbitrarily. We assume that the solution to (1) exists and is unique on all finite intervals. Under these assumptions, x and y are continuous and piecewise C^1. The following result in [5] is needed.

Proposition 2.1: Assume that g is positively homogeneous, that is, $g(\alpha v) = \alpha g(v)$ for all $\alpha > 0$ and $v \in \mathbb{R}$. Then the generalized Duhem model (1), (2) is rate independent.

As a specialization of (1) and (2), the *rate-independent semilinear Duhem model* is given by

$$\dot{x}(t) = \begin{bmatrix}\dot{u}_+(t)I_n & \dot{u}_-(t)I_n\end{bmatrix} \times \left(\begin{bmatrix}A_+\\A_-\end{bmatrix}x(t) + \begin{bmatrix}B_+\\B_-\end{bmatrix}u(t) + \begin{bmatrix}E_+\\E_-\end{bmatrix}\right), \tag{3}$$

$$y(t) = Cx(t) + Du(t), \qquad x(0)=x_0, \quad t\geq 0, \tag{4}$$

where $A_+ \in \mathbb{R}^{n\times n}$, $A_- \in \mathbb{R}^{n\times n}$, $B_+ \in \mathbb{R}^n$, $B_- \in \mathbb{R}^n$, $E_+ \in \mathbb{R}^n$, $E_- \in \mathbb{R}^n$, $C \in \mathbb{R}^{1\times n}$, $D \in \mathbb{R}$, and

$$\dot{u}_+(t) \triangleq \max\{0,\dot{u}(t)\}, \quad \dot{u}_-(t) \triangleq \min\{0,\dot{u}(t)\}. \tag{5}$$

Let the *limiting input-output map* $\mathcal{F}_\infty(u,y)$ be the set of points $z \in \mathbb{R}^2$ such that there exists an increasing, divergent sequence $\{t_i\}_{i=1}^\infty$ in $[0,\infty)$ satisfying $\lim_{i\to\infty} \|(u(t_i),y(t_i)) - z\| = 0$. A sufficient condition for the existence of the limiting periodic input-output map of a rate-independent semilinear Duhem model is given in [5].

The Dahl model [6] is the nonlinear friction model

$$\dot{F}(t) = \sigma \left|1 - \frac{F(t)}{F_{\mathrm{C}}}\mathrm{sgn}\,\dot{u}(t)\right|^{\gamma} \mathrm{sgn}\left(1 - \frac{F(t)}{F_{\mathrm{C}}}\mathrm{sgn}\,\dot{u}(t)\right)\dot{u}(t), \tag{6}$$

where F is the friction force, u is the relative displacement between the two surfaces in contact, $F_{\mathrm{C}} > 0$ is the Coulomb friction force, $\gamma \geq 0$ is a parameter that determines the force-deflection curve, and $\sigma > 0$ is the rest stiffness, that is, the slope of the force-deflection curve when $F = 0$.

The Dahl model (6) can be rewritten as

$$\dot{F}(t) = \sigma \begin{bmatrix}\mathcal{F}_+\big(F(t)\big) & \mathcal{F}_-\big(F(t)\big)\end{bmatrix} \begin{bmatrix}\dot{u}_+(t)\\ \dot{u}_-(t)\end{bmatrix}, \tag{7}$$

where

$$\mathcal{F}_+\big(F(t)\big) \triangleq \sigma \left|1 - \frac{F(t)}{F_c}\right|^{\gamma} \mathrm{sgn}\left(1 - \frac{F(t)}{F_c}\right), \tag{8}$$

$$\mathcal{F}_-\big(F(t)\big) \triangleq \sigma \left|1 + \frac{F(t)}{F_c}\right|^{\gamma} \mathrm{sgn}\left(1 + \frac{F(t)}{F_c}\right), \tag{9}$$

which is a generalized Duhem model for all $\gamma \geq 0$. Furthermore, since $\begin{bmatrix}\dot{u}_+(t) & \dot{u}_-(t)\end{bmatrix}^{\mathrm{T}}$ is positively homogeneous, Proposition 2.1 implies that (7) is rate independent for all $\gamma \geq 0$.

For the special case $\gamma = 1$, (6) becomes

$$\begin{aligned}\dot{F}(t) &= \sigma \left(1 - \frac{F(t)}{F_C}\mathrm{sgn}\,\dot{u}(t)\right)\dot{u}(t)\\ &= \begin{bmatrix}-\frac{\sigma}{F_C}F(t) + \sigma & \frac{\sigma}{F_C}F(t) + \sigma\end{bmatrix}\begin{bmatrix}\dot{u}_+(t)\\ \dot{u}_-(t)\end{bmatrix},\end{aligned}$$

which is a rate-independent semilinear Duhem model.

The *LuGre model* [7], which models the asperities of two surfaces as elastic bristles, is given by

$$\dot{x}(t) = \dot{u}(t) - \frac{|\dot{u}(t)|}{r\big(\dot{u}(t)\big)}x(t), \tag{10}$$

$$F(t) = \sigma_0 x(t) + \sigma_1 \dot{x}(t) + \sigma_2 \dot{u}(t), \tag{11}$$

where x is the average deflection of the bristles, u is the relative displacement, F is the friction force, and $\sigma_0, \sigma_1, \sigma_2 > 0$ are stiffness, damping, and viscous friction coefficients, respectively. Various choices for the function $r(\dot{u}(t))$ are given in [1, p. 83]. In [7] $r(\dot{u}(t))$ is defined by

$$r(\dot{u}(t)) = \frac{F_{\mathrm{C}}}{\sigma_0} + \frac{F_{\mathrm{S}} - F_{\mathrm{C}}}{\sigma_0}e^{-(\dot{u}(t)/v_{\mathrm{S}})^2}, \tag{12}$$

where $F_{\mathrm{C}} > 0$ is the Coulomb friction force, F_{S} is the stiction (sticking friction) force, and v_{S} is the Stribeck velocity, which is the velocity at which the steady state friction force starts decreasing.

The Dahl model is basically Coulomb friction with a lag in the change of the friction force when the direction of motion reverses. The Lugre model combines the friction lag of the Dahl model with the Stribeck effect, in which the friction force decreases at low magnitudes of velocity [4]. The state equations (10) and (11) can be rewritten as

$$\dot{x}(t) = \begin{bmatrix}1 & x(t)\end{bmatrix}\begin{bmatrix}\dot{u}(t)\\ -\frac{|\dot{u}(t)|}{r\big(\dot{u}(t)\big)}\end{bmatrix}, \tag{13}$$

$$y(t) = \sigma_0 x(t) + \sigma_1 \dot{x}(t) + \sigma_2 \dot{u}(t), \tag{14}$$

which is a generalized Duhem model of the form (1). Since r given in (12) is not positively homogeneous, the LuGre model is not necessarily rate independent.

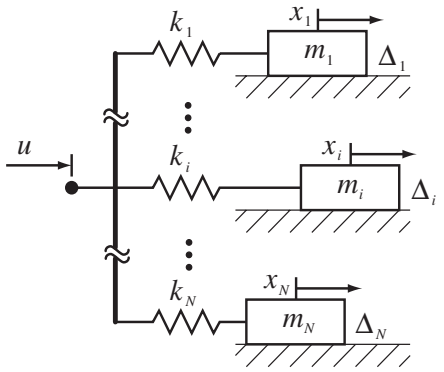

Fig. 1. The Maxwell slip model with N masses and N springs. Each mass is associated with a displacement deadband Δ_i, below which the mass does not move, and above which the mass moves with the same velocity as the common termination point.

The *Maxwell-slip model* [8]–[10] as shown in Figure 1, has N masses m_i with displacement x_i connected by a stiffness k_i to a common termination point whose displacement is u. Associated with each mass is a displacement deadband of width $\Delta_i \in \mathbb{R}$, below which the mass does not move, and above which the mass moves with velocity $\dot{u}$, that is, the inertia of the masses is ignored when the mass is sliding. We can write this system as the Duhem model

$$\dot{x}_i(t) = \begin{bmatrix}\mathcal{M}\big(x_i(t),u(t),\Delta\big) & 1\text{–}\mathcal{N}\big(x_i(t),u(t),\Delta\big)\end{bmatrix}\begin{bmatrix}\dot{u}_+(t)\\ \dot{u}_-(t)\end{bmatrix} \tag{15}$$

$$F(t) = \textstyle\sum_{i=1}^N k_i\big(-x_i(t) + u(t)\big), \tag{16}$$

for $i = 1,\ldots,N$, where F is the friction force, $\Delta \triangleq [\Delta_1 \cdots \Delta_N]$,

$$\mathcal{M}\big(x_i,u,\Delta\big) \triangleq U\big(-x_i + u - \Delta_i\big), \tag{17}$$

$$\mathcal{N}\big(x_i,u,\Delta\big) \triangleq U\big(-x_i + u + \Delta_i\big), \tag{18}$$

and,

$$U(v) \triangleq \begin{cases}1, & v \geq 0,\\ 0, & v < 0.\end{cases} \tag{19}$$

The Maxwell-slip model (15), (16) is a generalized Duhem model of the form (1), (2). Note that $\begin{bmatrix}\dot{u}_+(t) & \dot{u}_-(t)\end{bmatrix}^{\mathrm{T}}$ is positively homogeneous, and thus Proposition 2.1 implies that (15), (16) is rate independent.

TABLE I

CLASSIFICATION AND PROPERTIES OF FRICTION MODELS. ALL OF THESE FRICTION MODELS ARE DUHEM MODELS, WHICH SUGGESTS A DIRECT CONNECTION BETWEEN FRICTION AND HYSTERESIS.

Friction Model		Duhem type	Rate dependence	Continuity
Dahl	$0 \leq \gamma < 1$	generalized	rate independent	continuous, but not Lipschitz
	$\gamma = 1$	semilinear	rate independent	Lipschitz
	$\gamma > 1$	generalized	rate independent	Lipschitz
LuGre		generalized	rate dependent	Lipschitz
Maxwell-slip		generalized	rate independent	discontinuous

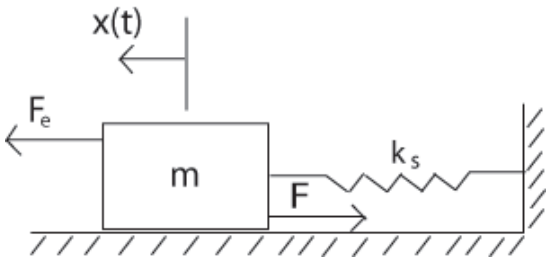

Fig. 2. Mass-spring system with friction force F and external force F_e.

III. BEHAVIOR OF A MASS-SPRING SYSTEM UNDER FRICTION

In order to study hysteresis caused by friction, we now consider the case in which one end of the spring is fixed and a force is exerted on the mass as shown in Figure 2. The system dynamics can be written as

$$\ddot{x}(t) + \frac{k_s}{m}x(t) = \frac{1}{m}F_e(t) - \frac{1}{m}F(x(t), \dot{x}(t)), \qquad (20)$$

where $x(t)$ is the displacement of the mass, k_s is the spring constant, m is the mass, $F_e(t)$ is the external force exerted on the mass, and $F(x(t), \dot{x}(t))$ is the friction force acting on the mass. The external force was chosen to be $F_e(t) = \sin(0.1t)$ N.

The velocity $\dot{x}(t)$ of the mass and the hysteresis map between external force F and displacement $x(t)$, generated with the Dahl, LuGre and the Maxwell-slip models are shown in Figures 7, 8, and 9, respectively.

All the three friction models exhibit hysteresis when incorporated into a mass-spring system as shown in Figures 7(b), 8(b), and 9(b).

IV. EXPERIMENTAL SETUP

We now describe an experimental setup for studying the effects of gearbox friction on the dynamics of a dc motor. The experimental setup is shown in Figure 6. A schematic of the setup is shown in Figure 7. Two cables are wound around the motor shaft and connected to load cells L_1 and L_2 that measure the force exerted by the springs k_1 and k_2. The dynamics of the shaft are given by,

$$I\ddot{\theta} = T_m - T_f + F_2 r - F_1 r, \qquad (21)$$

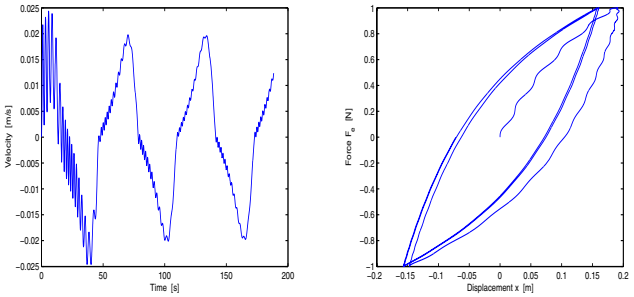

(a) (b)

Fig. 3. (a) Velocity $\dot{x}(t)$ of the mass and (b) the hysteresis map between the external force $F_e(t)$ and the displacement $x(t)$ of the mass for the mass-spring system (20), with the Dahl model, where $F_C = 0.75$ N, $\gamma = 1$, $\sigma = 7.5$ N/m, $k_s = 2$ N/m, $m = 1$ kg, and $F_e(t) = \sin(0.1t)$ m.

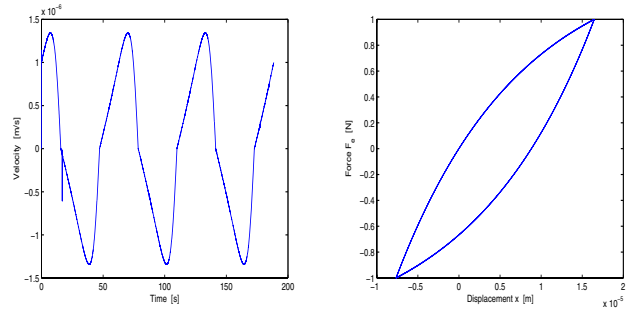

(a) (b)

Fig. 4. (a) Velocity $\dot{x}(t)$ of the mass and (b) the hysteresis map between the external force $F_e(t)$ and the displacement $x(t)$ of the mass for the mass-spring system (20), with the LuGre model (10), (11), where $F_C = 1$ N, $F_S = 1.5$ N, $v_S = 0.001$ m/s, $\sigma_0 = 10^5$ N/m, $\sigma_1 = \sqrt{10^5}$ N-s/m, $\sigma_2 = 0.4$ N-s/m, $k_s = 2$ N/m, $m = 1$ kg, and $F_e(t) = \sin(0.1t)$ m/s.

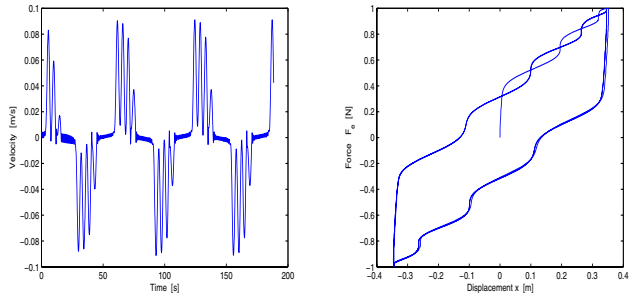

(a) (b)

Fig. 5. (a) Velocity $\dot{x}(t)$ of the mass and (b) the hysteresis map between the external force $F_e(t)$ and the displacement $x(t)$ of the mass for the mass-spring system (20), with the Maxwell-slip model, where N=10, Δ=$[1.5, 2.4, 3.3, 4.2, 5.1, 6, 6.9, 7.8, 8.7, 9.6] \times 10^{-3}$ m, k= $[1, 1.8, 2.6, 3.4, 4.2, 5, 5.8, 6.6, 7.4, 8.2]$ N/m, $m = 1$ kg, $k_s = 2$ N/m, and $F_e(t) = \sin(0.1t)$ m/s.

where θ is the angle of rotation of the shaft, I is the shaft moment of inertia, T_m is the torque exerted by the motor, T_f is the torque due to friction, r is the radius of the shaft, and F_1 and F_2 are the forces exerted on the shaft by the springs. The cables are wound such that, when the shaft rotates counterclockwise, F_1 increases and F_2 decreases. The springs are pre-stressed so that neither spring slacks while

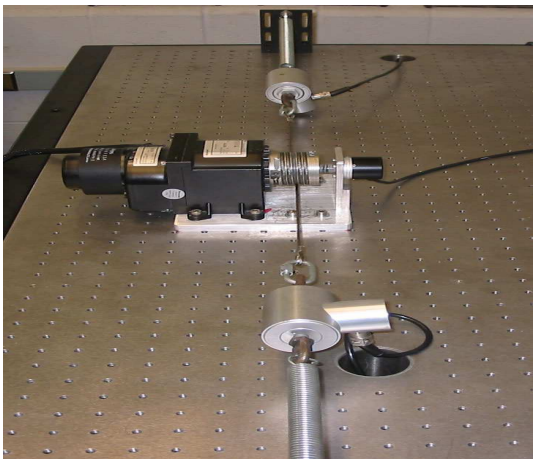

Fig. 6. Experimental setup for studying the effects of gearbox friction on the dynamics of a dc motor.

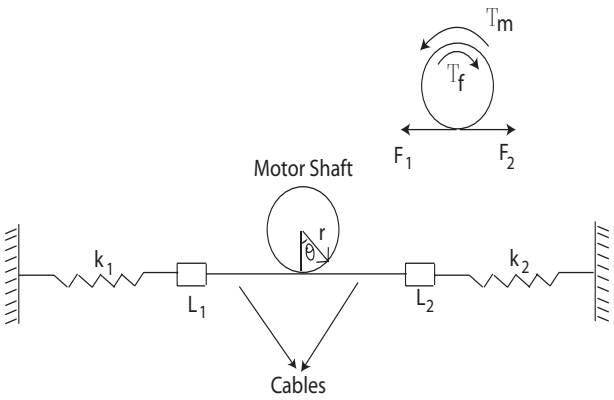

Fig. 7. Schematic of the experimental setup.

the shaft rotates in either direction. Let f_1 and f_2 be the initial force values and δ_1 and δ_2 be the deflections in the two springs, then

$$F_1 = f_1 + k_1\delta_1, \quad F_2 = f_2 + k_2\delta_2,$$

and

$$\delta_1 = r\theta, \quad \delta_2 = -r\theta.$$

Hence,

$$I\ddot{\theta} = T_m - T_f - (f_1 - f_2)r - (k_1 + k_2)r^2\theta. \tag{22}$$

The motor torque T_m is assumed to be proportional to the motor current, that is,

$$T_m = k_m i_m, \tag{23}$$

where k_m is the proportionality constant and i_m is the motor current. Hence, (22) becomes

$$\ddot{\theta}(t) + \frac{(k_1 + k_2)r^2}{I}\theta(t) = \frac{k_m}{I}i_m(t) - \frac{1}{I}T_f - \frac{(f_1 - f_2)r}{I}. \tag{24}$$

Note that the dynamics in (24) are same as the dynamics of the mass-spring system (20), if $\frac{k_s}{m} = \frac{(k_1+k_2)r^2}{I}$, $\frac{F_e}{m} = \frac{k_m}{I}i_m$, $\frac{F}{m} = \frac{1}{I}T_f$, and if symmetry is assumed, that is, if $f_1 = f_2$. The setup is connected to a digital computer through a dSpace 1103 system, which has 1 encoder, 5 A/D channels, and 5 D/A channels. Readings from the two load cells are amplified using an Endevco Voltage Amplifier Model 136. The load cells can take a maximum load of 75 Kg and have a sensitivity of 0.26 mV/Kg. The amplifier gain can be set anywhere between 0 and 1000, and the amplified signals are sampled by the dSpace system. The dc motor has a built-in tachometer that measures the angular rate of the motor shaft. The angular rate signal is read through an A/D channel. A Heidenhain encoder measures the angular deflection of the motor shaft. Current is supplied to the dc motor through a Quanser linear current amplifier LCAM. The required current profile is commanded to the current amplifier through one of the D/A channels. The amplifier provides a voltage signal proportional to the current supplied to the dc motor. This voltage is read through one of the A/D channels.

V. Simulation Results

In this section we simulate the dc motor dynamics given by (24). The friction torque T_f is modeled using the Dahl, LuGre, and Maxwell-slip models. The parameter values are $k_1 = k_2 = 10$ N/m, $f_1 = f_2 = 0.01$ N, $r = 1$ inch, and $k_m = 20$ N-m/A. Symmetry is assumed for simplicity. Assuming that the motor shaft is cylindrical and has a mass of $m = 2$ kg, its moment of inertia can be evaluated as $I = mr^2/2 = 4 \times 10^{-4}$ kg-m^2.

Firstly, for the Dahl friction model, with a motor current of $i_m(t) = 0.1\sin(0.1t)$ A, the angular deflection θ and the angular velocity $\dot{\theta}$ of the shaft are shown in Figure 12. The hysteresis map between the motor torque and the angular deflection is shown in Figure 13.

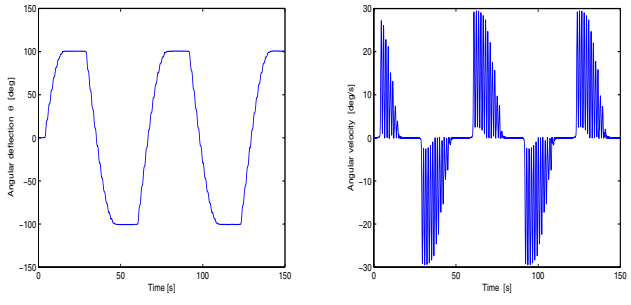

(a) (b)

Fig. 8. (a) Angular deflection θ and (b) angular velocity $\dot{\theta}$ of the motor shaft with the Dahl friction model, where $F_C = 0.75$ N-m, $\gamma = 1$, $\sigma = 7.5$ N-m/deg, and $i_m(t) = 0.1\sin(0.1t)$ A.

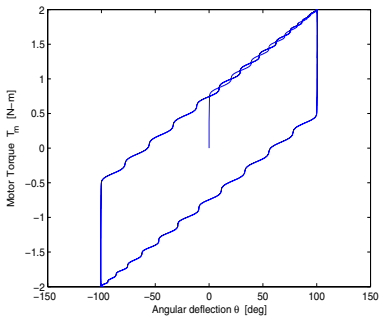

Fig. 9. Hysteresis map between the motor torque T_m and the angular deflection θ with the Dahl friction model, where $F_{\rm C} = 0.75$ N-m, $\gamma = 1$, $\sigma = 7.5$ N-m/deg, and $i_m(t) = 0.1\sin(0.1t)$ A.

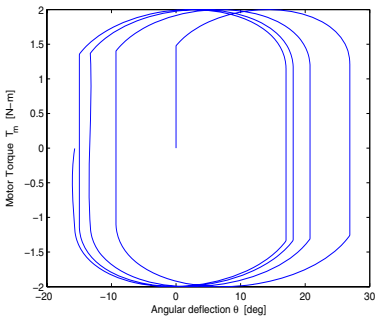

Fig. 11. Hysteresis map between the motor torque T_m and the angular deflection θ with the LuGre friction model, where $F_{\rm C} = 1$ N-m, $F_{\rm S} = 1.5$ N-m, $v_{\rm S} = 0.001$ deg/s, $\sigma_0 = 10^5$ N-m/deg, $\sigma_1 = \sqrt{10^5}$ N-m-s/deg, $\sigma_2 = 0.4$ N-m-s/deg, and $i_m(t) = 0.1\sin(0.1t)$ A.

For the LuGre and Maxwell-slip models, with a motor current of $i_m(t) = 0.1\sin(0.1t)$ A, the angular deflection θ and the angular velocity $\dot{\theta}$ of the shaft are shown in Figures 14 and 16, respectively. The corresponding hysteresis maps between the motor torque and the angular deflection are shown in Figures 15 and 17.

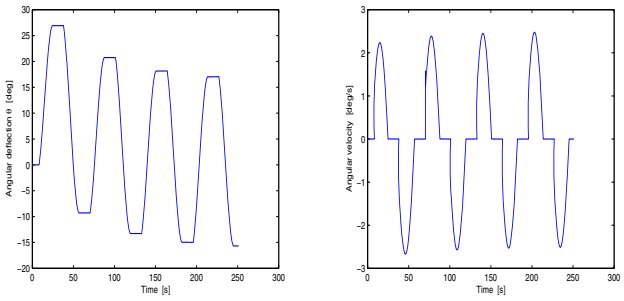

(a) (b)

Fig. 10. (a) Angular deflection θ and (b) angular velocity $\dot{\theta}$ of the motor shaft with the LuGre friction model, where $F_{\rm C} = 1$ N-m, $F_{\rm S} = 1.5$ N-m, $v_{\rm S} = 0.001$ deg/s, $\sigma_0 = 10^5$ N-m/deg, $\sigma_1 = \sqrt{10^5}$ N-m-s/deg, $\sigma_2 = 0.4$ N-m-s/deg, and $i_m(t) = 0.1\sin(0.1t)$ A.

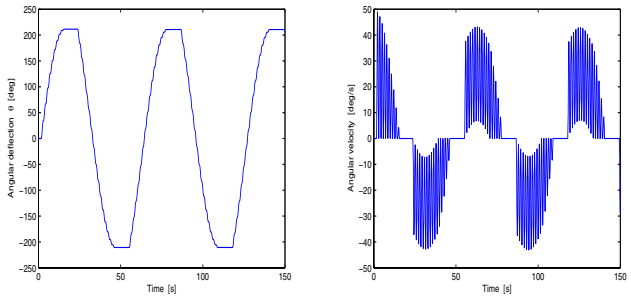

(a) (b)

Fig. 12. (a) Angular deflection θ and (b) angular velocity $\dot{\theta}$ of the motor shaft with the Maxwell-slip friction model, where $N = 10$, $\Delta = [1.5, 2.4, 3.3, 4.2, 5.1, 6, 6.9, 7.8, 8.7, 9.6] \times 10^{-3}$ deg, $k = [1, 1.8, 2.6, 3.4, 4.2, 5, 5.8, 6.6, 7.4, 8.2]$ N-m/deg, and $i_m = 0.1\sin(0.1t)$ A.

VI. Experimental Results

In this section we present and analyze the results obtained from the experimental setup described in Section 4. The current profile commanded to the current amplifier is $0.05\sin(0.2\pi t)$ A. The load cell readings, the actual current supplied by the amplifier to the dc motor, the angular velocity reading from the tachometer, and the angular deflection reading from Heidenhain encoder are shown in Figure 18. There is a bias in the current profile because of asymmetry in the setup, specifically the spring forces are not initially equal. Once the current supply is switched on, the motor shaft reaches an equilibrium position in which both the springs are equally stressed and then oscillates about that position. This behavior can be seen clearly in the load cell readings.

The motor shaft rotates to one side until the motor torque is more than the torque exerted by the springs and the grearbox friction, after which it stops rotating and stays motionless until the motor torque changes direction. This kind of motion is the reason for the occurrence of time intervals with zero shaft angular velocity as shown in the Figure 18. This behavior is consistent with what was observed in the simulations of the experimental setup as shown in Figures 12(b), 14(b), and 16(b). The angular velocity plot obtained from the experiment shown in Figure 18 matches best with the angular velocity plot obtained from the simulations using the LuGre friction model shown in Figure 14(b). Plot between the motor torque and the angular displacement exhibiting hysteresis in the experiment is shown in Figure 19. After initial transients, the plot settles down to a closed hysteresis loop. This hysteresis plot matches well with the one obtained from simulations using the LuGre friction model shown in Figure 15.

VII. Conclusion

In this paper we recast the Dahl, LuGre, and Maxwell-slip models as extended, generalized, or semilinear Duhem models. We classified each model as either rate independent or rate dependent. Smoothness properties of the three friction models were also considered.

We then studied the hysteresis induced by friction in single-degree-of-freedom systems. For each friction model, we computed the corresponding hysteresis map. Next we

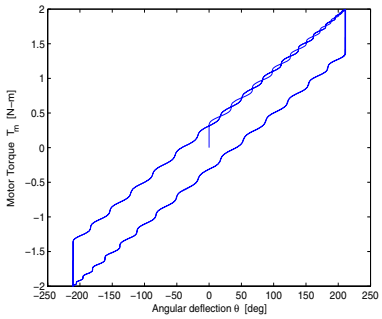

Fig. 13. Hysteresis map between the motor torque T_m and the angular deflection θ with the Maxwell-slip friction model, where $N = 10$, $\Delta = [1.5, 2.4, 3.3, 4.2, 5.1, 6, 6.9, 7.8, 8.7, 9.6] \times 10^{-3}$ deg, $k = [1, 1.8, 2.6, 3.4, 4.2, 5, 5.8, 6.6, 7.4, 8.2]$ N-m/deg, and $i_m = 0.1 \sin(0.1t)$ A.

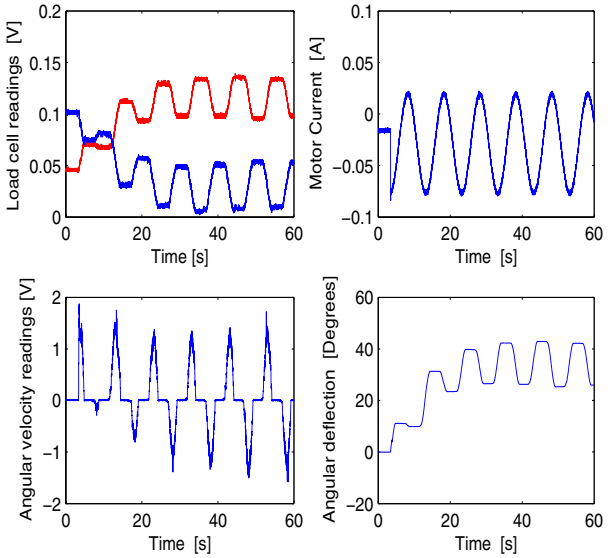

Fig. 14. Clockwise from top left, load cell readings, current supplied by the amplifier, the angular deflection, and the angular velocity readings for the dc motor experiment. Note that the angular velocity plot is similar to the plot in Figure 14(b).

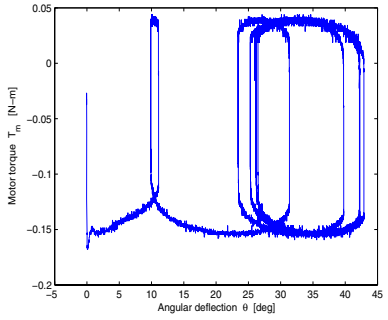

Fig. 15. Hysteresis map between the motor torque and the angular deflection for the dc motor experiment. Note that the hysteresis map is similar to the one in Figure 15.

developed a dc servo motor testbed and performed simple motion experiments on it. We then modeled the testbed dynamics and simulated them. By comparing the simulated and experimental results, it was found that the LuGre friction model provides the best model of the gearbox friction characteristics. The reason could be that the LuGre model exhibits the Stribeck effect where as the other two friction models do not.

REFERENCES

[1] B. Armstrong-Hélouvry, *Control of Machines with Friction*. Boston, MA: Kluwer, 1991.

[2] B. Armstrong-Hélouvry, P. Dupont, and C. C. de Wit, "A survey of model, analysis tools and compensation methods for the control of machines with friction," *Automatica*, vol. 30, no. 7, pp. 1083–1138, 1994.

[3] B. Feeny, A. Guran, N. Hinrichs, and K. Popp, "Historical review on dry friction and stick-slip phenomena," *Applied Mechanics Reviews*, vol. 51, no. 5, pp. 321–341, 1998.

[4] J. Oh, A. Padthe, and D. S. Bernstein, "Duhem models for hysteresis in sliding and presliding friction," in *Proc. IEEE Conf. Dec. Contr.*, Seville, Spain, December 2005.

[5] J. Oh and D. S. Bernstein, "Semilinear Duhem model for rate-independent and rate-dependent hysteresis," *IEEE Trans. Autom. Contr.*, vol. 50, no. 5, pp. 631–645, 2005.

[6] P. Dahl, "Solid friction damping of mechanical vibrations," *AIAA J.*, vol. 14, no. 2, pp. 1675–82, 1976.

[7] C. Canudas de Wit, H. Olsson, K. J. Åstrom, and P. Lischinsky, "A new model for control of systems with friction," *TAC*, vol. 40, no. 3, pp. 419–425, 1995.

[8] D. D. Rizos and S. D. Fassois, "Presliding friction identification based upon the Maxwell slip model structure," *Chaos*, vol. 14, no. 2, pp. 431–445, 2004.

[9] F. Al-Bender, V. Lampaert, and J. Swevers, "Modeling of dry sliding friction dynamics: From heuristic models to physically motivated models and back," *Chaos*, vol. 14, no. 2, pp. 446–445, 2004.

[10] F. Al-Bender, V. Lampaert, S. D. Fassois, D. D. Rizos, K. Worden, D. Engster, A. Hornstein, and U. Parlitz, "Measurement and identification of pre-sliding friction dynamics," in *Nonlinear Dynamics of Production Systems*. Weinheim: Wiley, 2004, pp. 349–367.

[11] J. Swevers, F. Al-Bender, C. G. Ganseman, and T. Prajogo, "An integrated friction model structure with improved presliding behavior for accurate friction compensation," *IEEE Trans. Autom. Contr.*, vol. 45, no. 4, pp. 675–686, 2000.